NON-INTRUSIVE DETERMINATION OF TURBULENT ENERGY BALANCE IN FREE AND CONFINED JET FLOWS

Sergey V. Alekseenko, Artur V. Bilsky, Vladimir M. Dulin,
Boris B. Ilyushin, Dmitriy M. Markovich
Institute of Thermophysics, Siberian Branch of RAS
Lavrentyev Ave., 1, Novosibirsk, 630090, Russia,
dmark@itp.nsc.ru

ABSTRACT

On the basis of PIV measurements the estimation of turbulent kinetic energy balance is performed for free and impinging jets. Influence of external periodical forcing is studied. For correct calculation of differential characteristics the appropriate interpolation and derivative calculation schemes are applied. The complete set of statistical moments as well as terms of momentum balance are obtained for studied flows.

INTRODUCTION

The necessity of developing new mathematical models for complex turbulent flows assumes the comprehensive experimental information to be retrieved. This allows, from one side, to provide the basic correlations for models closure research, and from the other side, to exploit the large data arrays for models verification. Some models for second-order closures (models for pressure-gradient – velocity correlation or dissipation) are already comprehensively tested and satisfactorily describe a number of simple flows. At the same time, for adequate description of more complex flows, such as impinging jets, more advanced models are usually applied and they require more deep information about the flow structure (triple statistical moments, differential characteristics such as turbulent energy dissipation rate etc.). Impinging jets are the hydrodynamic objects that are often used for the validation of CFD codes. This is because such flows are widespread in the industry (jet heating, cooling, drying) and nature (microbursts etc.).

The detailed experimental data on triple moments and differential characteristics are available only in few works even for simple enough flows. Thus, for free turbulent jet, the paper by Panchapakesan and Lumley (1993) could be mentioned as frequently referenced as well as several works of research groups of F. Hussein, I. Wygnanski and some other authors. For submerged impinging jets the two most cited articles of last decade contain a lot of information about flow structure – Cooper et al. (1993) and Nishino et al. (1996). Each experimental technique used in the aforementioned works (HWA, LDA, PTV) has its own principal restrictions and this fact did not allow authors to obtain comprehensive information. Thus, the direct calculation of dissipation rate is impossible for single-point techniques and this quantity is usually determined only as residual term in energy balance equation by adding different assumptions.

Particle Image Velocimetry is one of the most modern non-intrusive methods for flow diagnostics. The possibility of instant measurements of spatial velocity distributions allows to obtain a wide spectrum of characteristics – spatial velocity derivatives, correlations etc. Besides, experimental PIV data can be directly utilized for comparison with results of LES modeling. However for correct calculation of above-mentioned quantities it is necessary to elaborate a number of post-processing procedures such as the proper data validation methods, the approaches for interpolation of velocity fields which is caused by removal of spurious vectors. Also appropriate differencing schemes assuming physically justified balance between low-pass and high-pass filtering have to be developed.

The present work is devoted to the experimental study of hydrodynamic structure of axisymmetric free and impinging jet flows using PIV. Main emphasis has been done on the correct calculation of spatial velocity derivatives and estimation of turbulent kinetic energy balance.

INTERPOLATION PROCEDURE

When instantaneous velocity vector field measured by PIV is validated and spurious vectors are removed, the holes have to be interpolated in order to allow the vector field derivatives computation. Spurious vectors won't always be isolated from each other, and in some cases constitute the clusters, which also need to be interpolated.

In the present paper the study of interpolation procedure is restricted to the finite impulse response linear filters. Interpolation was implemented independently for each velocity component, using Taylor series expansions for velocity component $U_{i,j}$:

$$U_{i,j} = \sum_{k,l=0}^{\infty} \frac{i^k j^l}{k!\,l!} \frac{\partial^{k+l} U}{\partial x^k \partial y^l}\bigg|_{0,0} (\Delta x)^k (\Delta y)^l \qquad (1)$$

where Δx and Δy are the grid spacing, i and j are the node indices, $(0,0)$ – coordinates of the node to be interpolated. Using equation (1) for nodes closest to the one being interpolated, interpolation filter can be estimated using the following equation:

$$U_{0,0} = \frac{1}{a}\sum_{i,j} a_{i,j} U_{i,j} + \sum_{i+j=n+1}^{\infty} \alpha_{i,j} \frac{\Delta x^i \Delta y^j}{i!\,j!} \frac{\partial^{i+j} U}{\partial x^i \partial y^j}\bigg|_{0,0} + \varepsilon\sigma_U a \quad (2)$$

where a and $\alpha_{i,j}$ are given by:

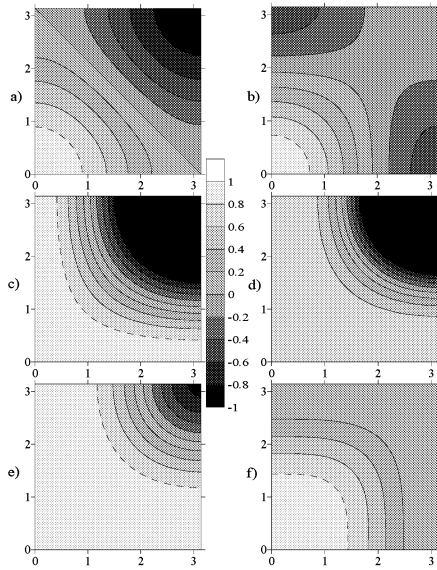$$a = \sum_{i,j} a_{i,j} \quad \text{and} \quad \alpha_{i,j} = \frac{1}{a}\sum_{l,m} a_{l,m} l^i m^j \qquad (3)$$

Figure 2. Frequency amplitude response of a) "I1", b) "B", c) "I2", d) "A", e) "C", and f) "D" filters versus $k_x\Delta x$ and $k_y\Delta y$.

The values $a_{i,j}$ are obtained using equations (1). The second term at the right-hand side of (2) is the truncation error and the last term is the uncorrelated noise error (Hamming, 1998). σ_U is the measurement noise level, and the noise amplification coefficient (ε) can be obtained by:

$$\varepsilon^2 = \frac{1}{a^2}\sum_{i,j} a_{i,j}^2 \qquad (4)$$

Truncation error decreases when the order of filter and noise amplification increases. So, the compromise should be found between these two sources of uncertainty taking into account that use of high order filters requires longer computation time.

In the present paper the study of interpolation filters is restricted by 3x3 linear filters. Figure 1 shows impulse response of the studied filters.
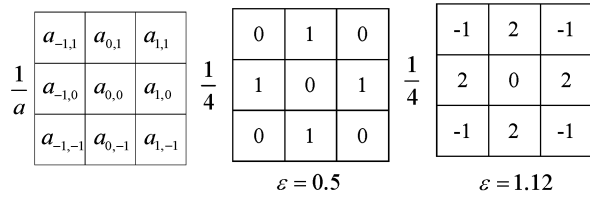

Figure 1. Nomenclature (left) for the impulse response of linear filters. Impulse response for the interpolating filters "I1" (center) and "I2" (right).

The first filter labeled as "I1" is of the second order, the second one, labeled as "I2", is of the third order. Frequency response of these filters can be represented using transfer function. Transfer function due to the truncation is given by the following equation:

$$Tr = \frac{U_{meas.}}{U_{true}} = 1 - \frac{\sum_{i+j=n+1}^{\infty} \alpha_{i,j} \frac{\Delta x^i \Delta y^j}{i!\,j!} \frac{\partial^{i+j}U}{\partial x^i \partial y^j}\Big|_{0,0}}{U_{true}} \qquad (5)$$

Index "meas." means estimated velocity component using interpolating filter. Replacement of U_{true} by Fourier mode $U_{true}=u\exp(i(k_x x + k_y y))$ gives the low pass filter:

$$Tr = \frac{1}{a}\sum_{i,j=0} a_{i,j}\cos(i\Delta x k_x)\cos(j\Delta y k_y) \qquad (6)$$

where k_x and k_y are the spatial wave numbers. Transfer function due to the noise can be expressed as:

$$Tn = 1 - \frac{\varepsilon\sigma_U}{u} \qquad (7)$$

Total transfer function $T=TrTn$ for filters "I1", "I2" in comparison with 5x5 filters "A", "C" and "D" reported by Nogueira et al. (1997) are presented in Figure 2. The level of measurement noise was equal to 0.03. Filter marked as "B" is a 3x3 moving average filter. It can be noticed that filters referred to as "I1" and "B" have quite small area where signal is recovered with uncertainty less than 20% (shown by dashed line), so these schemes were rejected. Filter "C" is obtained using filter "A", assuming minimization of noise amplification coefficient (Nougueira et al., 1997), and as can be seen from Fig. 2, it has better frequency response. Because the filters "C" and "D" are built for use in iterative interpolation they were rejected. Most suitable with mentioned criteria, filter "I2" was chosen to be used for interpolation. Interpolation equations for vectors located at the measurement area boundary were obtained using similar approach.

DERIVATIVE COMPUTATION PROCEDURE

Derivative filters were studied in a similar manner with interpolation filters. Proper selection of the finite-difference scheme is the aim of the present part of paper. Detailed study of derivative linear lifters application for PIV can be found in Foucaut and Stanislas (2002).

Centered difference scheme can be estimated by following equation:

$$\frac{\partial U}{\partial x}(x_j) = \frac{1}{a\Delta x}\sum_{i=1}^{n/2} a_i(U_{j+i} - U_{j-i})$$

$$+ \sum_{i=n+1}^{\infty} \alpha_i \frac{\Delta x^{i-1}}{i!}\frac{\partial^i U}{\partial x^i}(x_j) + \varepsilon\frac{\sigma_U}{\Delta x} \qquad (8)$$

where:

$$a = 2\sum_{i=1}^{n/2} ia_i \;;\; \alpha_i = \frac{2}{a}\sum_{l=1}^{n/2} a_l l^i \cdot \qquad (9)$$

Characteristics of the centered difference filters are presented in Table 1, a). As expected, truncation error decreases and noise amplification increases when the order of filter increases.

Compact difference schemes also studied by Foucaut and Stanislas (2002) are given by

$$\beta U''_{j-2} + \chi U''_{j-1} + U''_j + \chi U''_{j+1} + \beta U''_{j+2} =$$

$$c\frac{U_{j+3}-U_{j-3}}{6\Delta x} + b\frac{U_{j+2}-U_{j-2}}{4\Delta x} + a\frac{U_{j+1}-U_{j-1}}{2\Delta x} \qquad (10)$$

where parameters β, χ, a, b, c obtained using Taylor series are presented in Table 1, c). The compact difference schemes seem to be interesting because of lower noise amplification coefficient for higher orders in comparison with centered difference schemes.

Table 1. Characteristics of: a) centered difference schemes; b) Richardson extrapolation schemes, * – indicates that coefficients are obtained by means of ε minimization; c) compact difference schemes.

a) Centered difference schemes

n	a	a_1	a_2	a_3	a_4	α_{n+1}	ε
2	2	1	0	0	0	1	0.71
4	12	8	-1	0	0	4	0.95

b) Richardson extrapolation

n	a	a_1	a_2	a_3	a_4	α_{n+1}	ε
2	1	1	0	0	0	1	0.71
4	3	4	-1	0	0	4	0.95
2*	65	1	0	0	64	63.	0.09
4*	1239	272	1036	0	-69	214.	0.33

c) Compact difference schemes

n	a	b	c	χ	β	α_{n+1}	ε
6	1.(5)	0.(1)	0	0.(3)	0	4	1
8	1.48	0.46	0	0.(4)	0.03	46	0.9

For low-frequency signal the noise is the principal source of error. To minimize noise amplification coefficient the Richardson extrapolation based on the linear combination of the centered difference schemes with different data spacing can be used:

$$\frac{\partial U}{\partial x}(x_j) = \frac{1}{a} \sum_{i=1,2,4,8} \frac{a_i(U_{j+i} - U_{j-i})}{2i\Delta x}$$

$$+ \sum_{i=n+1}^{\infty} \alpha_i \frac{\Delta x^{i-1}}{(n+1)!} \frac{\partial^i U}{\partial x^i}(x_j) + \varepsilon \frac{\sigma_U}{\Delta x} \tag{11}$$

where coefficients a_i are parameters to be optimized. Characteristics of the mentioned schemes are presented in Table 1, b).

An alternative least-square filter based on noise minimization was proposed by Raffel et al. (1998):

$$\frac{\partial U}{\partial x}(x_j) = \frac{-2U_{j-2} - U_{j-1} + U_{j+1} + 2U_{j+2}}{10\Delta x}$$

$$+ 3.4 \frac{\Delta x^2}{(3)!} \frac{\partial^3 U}{\partial x^3}(x_j) + 0.316 \frac{\sigma_U}{\Delta x} \tag{12}$$

Similar to interpolation filters analysis, the frequency response of the centered difference schemes for derivative filters can be estimated using transfer function $T=TnTr$, where:

$$Tn = 1 - \frac{\varepsilon \sigma_U}{\Delta x \left(\partial U / \partial x\right)_{true}} = 1 - \frac{\varepsilon \sigma_U}{k\Delta x} \tag{13}$$

$$Tr = \frac{\left(\partial U / \partial x\right)_{est}}{\left(\partial U / \partial x\right)_{true}} = 1 - \frac{\sum_{i=n+1}^{\infty} \alpha_i \frac{\Delta x^i}{i!} \frac{\partial^i U}{\partial x^i}}{\left(\partial U / \partial x\right)_{true}} \tag{14}$$

Low pass filter due to the truncation (14) for centered difference schemes is expressed by (15), for compact difference schemes by (16) and for Richardson extrapolation by (17):

$$Tr = \frac{1}{ak\Delta x} \sum_{i=1}^{n/2} 2a_i \sin(ik\Delta x) \tag{15}$$
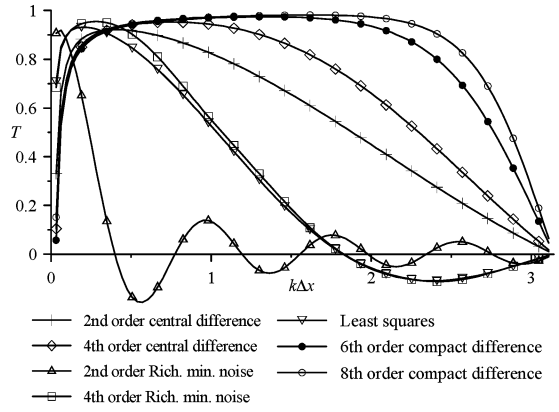

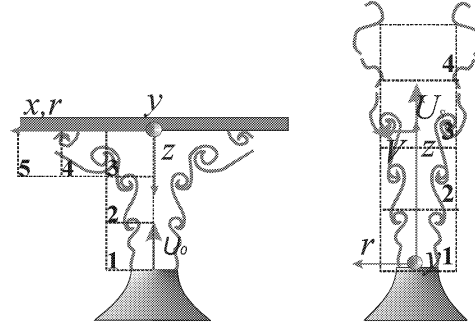Figure 3. Transfer function of derivative filters.

Figure 4. Sketch of impinging (left) and free jet (right).

$$Tr = \frac{\frac{1}{3} c \sin(3k\Delta x) + \frac{1}{2} b \sin(2k\Delta x) + a \sin(k\Delta x)}{(1 + 2\beta \cos(2k\Delta x) + 2\chi \cos(k\Delta x))k\Delta x} \tag{16}$$

$$Tr = \frac{1}{ak\Delta x} \sum_{i=1}^{n/2} \frac{a_i}{i} \sin(ik\Delta x) \tag{17}$$

As can be seen from Figure 3 the bandwidth and the lower cutoff frequency of the centered difference filters increase with the order of the filter. The compact difference filters give much wider bandwidth than the centered ones.

For noise minimized Richardson extrapolation filter, low and high cutoff frequencies are about several times lower than for compact filters. It can be noticed from Figure 3 that least squares scheme is similar to the 4th order noise minimization Richardson extrapolation. According to Foucaunt and Stanislas (2002) the most appropriate derivative scheme assumes that high cutoff frequency should be located where the noise becomes predominant and minimal noise amplification coefficient should be provided. In present study the least squares scheme proposed by Raffel et al. (1998) is chosen as optimal for application to PIV measurements without any optimization of the interrogation window size. Assuming 75% overlapping such approach provides good low frequency resolution together with low noise amplification.

EXPERIMENTAL SETUP

The experiments have been performed in a rectangular water tank facility. The water flow was driven by water pump which rotation speed was precisely controlled by an inverter. Water temperature was maintained constant using thermostat with $\pm 1^\circ C$ of

607

temperature variations. Both impinging and free submerged water jets were studied. To organize impinging jet flow the impingement plate was mounted into the water tank.

For impinging jet flow the diameter of nozzle exit was equal to 15 mm and Reynolds number was 7600; for free jet flow – 10 mm and 25000 correspondingly. The low-amplitude external excitation was applied with the frequency from most sensitive range for jet column. The frequency is characterized by Strouhal number $Sh = fd/U_0$ derived on the basis of nozzle diameter and velocity at the nozzle exit. Imposed perturbations have had an axisymmetric mode and affect the large-scale structures inside the jet shear layer.

For velocity field measurements Dantec PIV system was used, consisting of NewWave solo IV double cavity Nd:YAG laser, two HiSence 13 CCD cameras and Dantec 2500 PIV processor. Dantec Flow Manager software was used to operate PIV system. Sketches of both kinds of the flow are presented in Figure 4.

GOVERNING EQUATIONS

Both free and impinging jets have general axial symmetry and so can be described using cylindrical coordinate system. Jets have no average swirl, so that the azimuthal mean velocity and all correlations involving odd power of the azimuthal component can be assumed as zero.

Using axisymmetric conditions of flow, continuity equation is given by (18).

$$\frac{\partial V}{\partial r} + \frac{V}{r} + \frac{\partial U}{\partial z} = 0 \qquad (18)$$

Axial mean momentum transport is expressed as follows:

$$V\frac{\partial U}{\partial r} + U\frac{\partial U}{\partial z} + \frac{\partial(r\overline{\upsilon u})}{r\partial r} + \frac{\partial \overline{u^2}}{\partial z} + \frac{\partial P}{\rho \partial z} = 0 \qquad (19)$$

Turbulent kinetic energy budget equation is given by:

$$-\left(V\frac{\partial\langle k^2\rangle}{\partial r} + U\frac{\partial\langle k^2\rangle}{\partial z}\right) - \left(\frac{\partial\left(r\langle k^2\upsilon\rangle\right)}{r\partial r} + \frac{\partial\langle k^2 u\rangle}{\partial z}\right)$$

$$-\frac{1}{\rho}\left(\frac{\partial\left(r\langle p\upsilon\rangle\right)}{r\partial r} + \frac{\partial\langle pu\rangle}{\partial z}\right) + \qquad (20)$$

$$+\upsilon\left(\frac{\partial^2\left(r\langle k^2\rangle\right)}{r\partial r^2} + \frac{\partial^2\langle k^2\rangle}{\partial z^2}\right) - \left(\langle\upsilon^2\rangle\frac{\partial V}{\partial r} + \langle w^2\rangle\frac{V}{r} + \right.$$

$$\left. +\langle u^2\rangle\frac{\partial U}{\partial z} + \langle u\upsilon\rangle\left(\frac{\partial V}{\partial z} + \frac{\partial U}{\partial r}\right)\right) - \varepsilon = 0$$

$$k^2 = \frac{u_i u^i}{2} = \frac{\langle u^2 + \upsilon^2 + w^2\rangle}{2}, \quad \varepsilon = \varepsilon_{ii} \qquad (21)$$

First term at the left-hand side of equation (20) is convection (C). Second term indicates turbulent diffusion (D_T). Third and fourth terms correspond to the pressure (D_P) and viscous diffusion. Fifth and sixth terms indicate production (P_M) and viscous dissipation (ε). As expected in turbulent flows, away from the walls, the viscous diffusion is negligible in comparison with the turbulent contributions and hence will be neglected for both impinging and free jet (Nishino et al., 1996, Panchapakesan and Lumley, 1993). Pressure diffusion term can be neglected for free jet, but should be kept in balance equation for impinging jet.

Turbulent kinetic energy dissipation is the most challenging part to estimate in turbulence energy balance equation. The complete equation for viscous dissipation in Cartesian coordinates is:

$$\varepsilon_{ii} = v\left\langle 2\left(\frac{\partial\upsilon}{\partial x}\right)^2 + 2\left(\frac{\partial u}{\partial z}\right)^2 + 2\left(\frac{\partial u}{\partial z} + \frac{\partial\upsilon}{\partial x}\right)^2 \right.$$

$$\left. +\left(\frac{\partial\upsilon}{\partial z} + \frac{\partial u}{\partial x}\right)^2 + \left(\frac{\partial\upsilon}{\partial y} + \frac{\partial w}{\partial x}\right)^2 + \left(\frac{\partial u}{\partial y} + \frac{\partial w}{\partial z}\right)^2\right\rangle \qquad (22)$$

Due to specifics of one-plane PIV approach all the terms of (22) cannot be measured. Third term at the right-hand side of (22) is obtained using continuity equation. Fifth and sixth terms can be estimated with fourth one assuming micro scale pulsation isotropy. Similar approach for total dissipation estimation can be found in Piirto et al. (2003).

RESULTS AND DISCUSSION

Free Jet

During experiments the whole measurement area was separated into several regions (Figure 4, b). Measurements were performed both for unforced and forced jet conditions. For each region 3,000 instant velocity distributions have been obtained using iterative cross correlation algorithms. In free jet experiments the velocity vector fields were computed with 75% overlap (157x125 vectors) which corresponds to grid spacing 0.43 mm. This scale is approximately thirteen times higher than Kolmogorov lengthscale.

Using algorithms described above the instant fields of spatial derivatives have been calculated. Also the complete set of statistical moments up to 4th order has been obtained. PDF based filtration algorithm (Heinz et al., 2004) was applied in order to remove spurious velocity vectors. Distributions of statistical moments show good agreement between forced and unforced cases for far field of a jet and are very similar to results presented by Panchapakesan and Lumley (1993), further referred to as PL. Some exception is found for triple correlation of axial velocity. Value $<u^3>$ obtained both for forced and unforced jet has negative value in the vicinity of jet axis. The turbulent intensity of the azimuthal velocity and all its correlations are assumed to be equal to radial ones. Vindication of this assumption is done by PL.

Gradients of the third moments determine turbulent diffusion of kinetic energy, so they are important in estimation of the kinetic energy budget. The complete set of triple moments was also measured.

The axial mean momentum transport, neglecting viscous terms, was estimated. Pressure gradient is found as residual term in equation (19). It can be noticed, that behavior of momentum balance terms is similar for forced and unforced jets.

Terms of the turbulent kinetic energy budget are presented in Figure 5 in comparison with PL results. Scale factor U_s is the centerline mean velocity, L_u is local lengthscale taken to be dimensional half-width of the jet. As expected, the viscous diffusion term is negligible in comparison with other terms.

For both cases all the components of energy budget are quite close to PL results when accounting for some difference in boundary conditions including Reynolds number, working media etc. For flows far from the boundaries the pressure diffusion term can be assumed to be negligible. So Panchapakesan and Lumley (1993) found dissipation as a residual term in budget equation.

In the present study the dissipation was obtained in two ways. First one is the similar to PL approach, second one – dissipation was directly calculated from measured instant velocity fields. It is known (Piirto et al., 2003) that value of dissipation computed di-

rectly from PIV data depends on the overlapping rate, the derivative scheme used, and the interrogation area size. In the case of the same grid spacing, estimated dissipation is rather lower for 50% overlapping compared to the one measured without any overlap. Thus it is expected that 75% overlap used will lead to more underestimated value of dissipation. The comparison of two distributions of dissipation rate obtained with approaches described above has shown that estimated dissipation is 9.6 times lower than budget equation residual term. Estimated dissipation multiplied by 9.6 (symbols) is presented in Figure 5, d), together with residual term (curves). The dependences are in satisfactory agreement.

Impinging jet

In case of impinging jet study the whole measurement area was also separated into several regions (Fig.4, a). For each region 1500 vector fields were obtained both for forced and unforced jet conditions. The overlap of 75% was used, so the grid spacing was 0.13 mm that exceeds Kolmogorov lengtscale in 3.25 times.

Similar to the free jet case, the whole number of statistical moments up to 4th order has been calculated. The comparison of jet characteristics for forced and unforced conditions has been performed. It can be concluded from the measured distributions for whole averaging procedure that the mixing layer of the forced jet becomes wider and the level of RMS pulsations is substantially higher in comparison with the unforced case. Both distributions of skewness factor, characterising asymmetry of turbulent pulsations, and kurtosis, indicating the "spottiness" of the turbulent flow field, become more non-uniform when the forcing is applied. Besides, extremums of triple and fourth order moments shift from the area of free jet mixing layer towards to the regions where large powerful vortices interact with impingement wall. The behavior of Reynolds stresses is also similar to the one for higher statistical moments, however the pronounced extremes are also observed in the close vicinity of the nozzle exit where the generation of large-scale structures takes place.

Using assumption reported by Nishino et al. (1996) for turbulent intensity of azimuthal velocity fluctuations, axial mean momentum transport equation terms were obtained. Similar to free jet case the forcing does not lead to essential changes in axial mean momentum transport terms. Unlike free jet, diffusion terms for the impinging jet are close to zero in the vicinity of jet axis.

The terms of turbulent kinetic energy balance have been calculated both for forced and unforced impinging jet flow. Contrary to free jet, pressure diffusion term cannot be refused in turbulent kinetic energy balance equation for impinging jet case. Turbulent kinetic energy balance equation terms are shown in Figure 6 for unforced and forced jet conditions. The results for $z/d = 1$ cross-section are presented. It was found that viscous diffusion appeared to be negligible in that region, so this value was excluded from further consideration. The curves are normalized by U_0^3/d. For both cases the convection terms are very close to each other, turbulent diffusion terms have different values near jet axis. Productions terms, similarly to free jet case, have off-axis peaks corresponding to the center of jet shear layer. The dissipation terms, contrary to free jet, have extremes in the center of shear layer that is explainable for initial region of jet flow. It can be noticed that in forced jet case the dissipation and production terms have rather lower values than the same terms for unforced jet. Pressure diffusion obtained as residual term of budget equation has significant value and seems to be negative between shear layer and jet axis. In the outer shear layer area the pressure diffusion term appears to be positive.

Figure 7 presents exponential dependence obtained by Piirto et al. (2003) for 50% overlapping and 2nd order centered difference scheme. Similarly, the exponential law was applied for estimation of true value of dissipation in the case of impinging jet. As a basis the empirical coefficient obtained in free jet experiments was used. This coefficient represents the ratio between dissipation obtained as a residual term and the value directly calculated with account for 75% overlapping and using the least squares derivative scheme. This point is shown as an open circle in Fig. 6. Taking into account that the used spatial resolution exceeded Kolmogorov lenghtscale 3.2 times, it was found that the ratio between underestimated dissipation obtained experimentally and the true one is about 1.8. This coefficient is used for representation of dissipation profiles in Fig. 7,d.
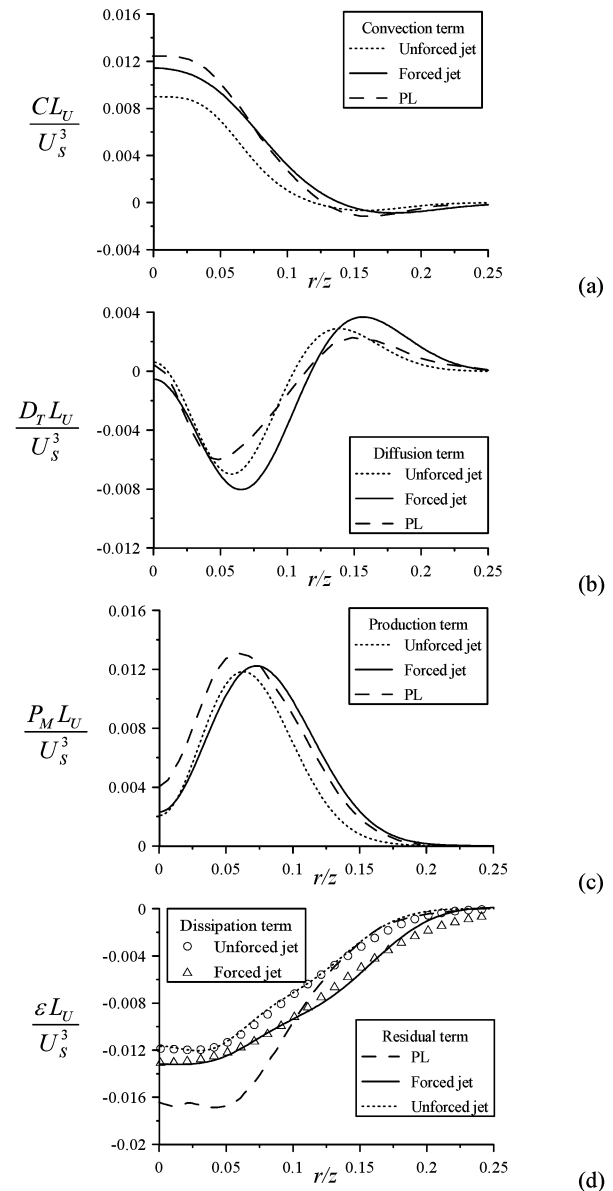

(a)

(b)

(c)

(d)

Figure 5. Turbulent kinetic energy balance equation terms. Free jet. Re = 25,000. Forced case: $z/d = 14$, Sh = 0.5. Unforced case: $z/d = 17$. PL: $z/d = 60$-120, Re = 11,000.
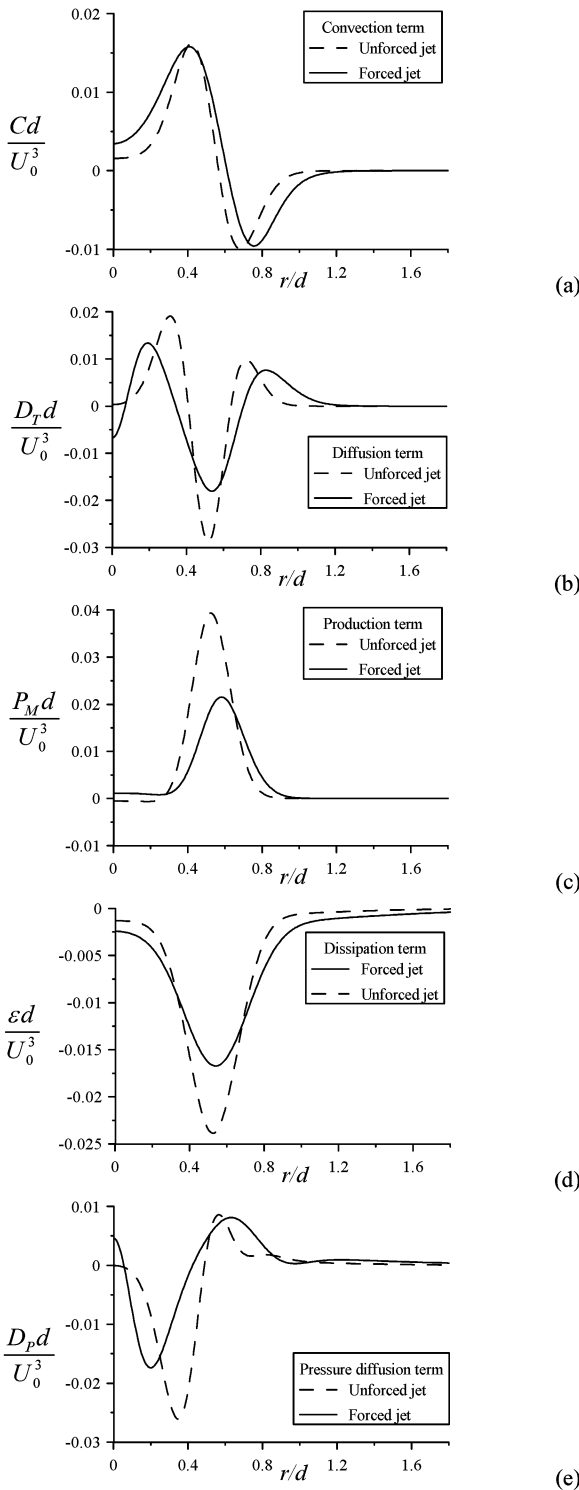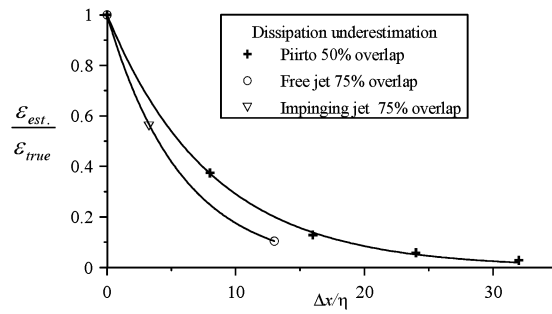
Figure 7. Dissipation underestimation profile versus grid spacing.

suitable filters were implemented in order to obtain spatial derivatives from PIV data. The complete set of statistical moments of velocity fluctuations are measured. The estimates of convection, diffusion and mean pressure gradient terms in axial mean momentum balance equation are computed. All terms of turbulent kinetic energy balance equations are directly estimated from PIV data, except for the pressure diffusion term. Taking into account the dependence of dissipation term estimate on spatial resolution, all the terms of turbulent energy equation balance are obtained in the case of impinging jet study where pressure diffusion is considered as residual term. In both flows the viscous terms are found to be negligible.

ACKNOLEDGMENTS

REFERENCES

Cooper, D., Jackson, D. C., Launder, B. E., Liao, G. X. 1993. Impinging jet studies for turbulence model assessment - I. Flow-field experiments. *Int. J. Heat Mass Transfer*, **36**, 2675-2684.

Foucaut, J. M. and Stanislas, M., 2002, "Some considerations on the accuracy and frequency response of some derivative filters applied to particle image velocimetry vector fields", *Meas. Sci. Technol.*, Vol. 13, pp. 1058-1071.

Hamming, R. W., 1989, "Digital filters", (Englewood Cliffs, NJ: Prentice-Hall).

Heinz, 0., Ilyushin, B., Markovich, D., "Application of a PDF based method for the experimental statistical processing of experimental data". *Int. J. Heat and Fluid Flow*, Vol. 25, pp. 864-874.

Nishino, K., Samada, M., Kasuya, K. and Torii, K., 1996, "Turbulence statistics in the stagnation region of an axisymmetric impinging jet flow", *Int. J. Heat and Fluid Flow*, Vol. 17, pp. 193-201.

Nogueira, J., Lecuona, A. and Rodrigues P. A., 1997, "Data validation, false vectors correction and derived magnitudes calculation on PIV data", *Meas. Sci. Technol.*, Vol. 9, pp. 1493-1501.

Panchapakesan, N. R., and Lumley, J. R., 1993, "Turbulence measurements in axisymmetric jets of air and helium. Part 1. Air jet", *Journal of Fluid Mechanics*, Vol. 246, pp. 197-223.

Piirto, M., Saarenrinne P., Eloranta H. and Karvinen, R., 2003, "Measuring turbulence energy with PIV in a backward-facing step flow", *Experiments in fluids*, Vol. 35, pp. 219-236.

Raffel, M., Willert C., and Kompenhans, J., 1998, "Particle image velocimetry", *A Practical Guide* (Berlin: Springer), pp. 147-71.

Figure 6. Turbulent kinetic energy balance equation terms. Impinging jet. $Re = 7,600$, $H/d = 3$, $z/d = 1$, for forced jet $Sh = 0.5$.

CONCLUSIONS

A turbulent round free and impinging jets are experimentally studied using PIV. The frequency response aspects for different interpolation and derivative linear filters are investigated. Most